DOI: 10.13009/EUCASS2017-68

Numerical modeling of continuous blowing surface in hypersonic boundary layers

Fabio Pinna⋆ and Fernando Miró Miró⋆⋆
⋆ Senior Research Engineer, von Karman Institute for Fluid Dynamics
Chaussée de Waterloo, 72, B-1640 Rhode-St-Genèse, Belgium
⋆⋆PhD Candidate, von Karman Institute for Fluid Dynamics
Chaussée de Waterloo, 72, B-1640 Rhode-St-Genèse, Belgium

6^{th} July 2017

Abstract

Hypersonic vehicles need to withstand high thermal loads during their mission. In case of very high energy flows ablative materials are used to build a Thermal Protection System (TPS). The outgassing due to the pyrolysis of the TPS directly affects the boundary layer stability. This paper studies the effect of wall blowing under controlled conditions, such as porous surfaces, and propose a model for a continuously blowing surface, thus mimicking the behavior of an ablative heat shield. The two models displays a similar shift to lower frequencies for the instabilities growth rate peak and an increased instability of the boundary layer.

1. Introduction

Hypersonic vehicles reentering from planetary missions or cruising in suborbital flights need to withstand high thermal loads due to the strong shock in front of the body and the high friction at the wall. A mishandling of the resulting aerodynamic heating can potentially endanger the mission, therefore a Thermal Protection System (TPS) is usually put in place. In case of very high energy flows ablative heat shields are usually preferred, dissipating most of the energy by means of pyrolysis and ablation. A direct effect of the heat flux imposed at the wall is the sublimation process, that produces an outgassing flow into the boundary layer. As a consequence the surface recedes along the wall normal. Material properties are irregularly distributed resulting in flow inhomogeneities; for this reason, small variations in the blowing velocities arise from the ablating surface, imposing tiny wall velocity perturbations. Such additional disturbances impact heavily the flow stability, potentially moving upstream the expected transition onset. If not correctly taken into account the premature laminar-to-turbulent transition can breed an unforeseen and drastic heat flux peak at the wall (see for instance Elison & Webb[4]), possibly leading to a catastrophic protection system failure. This worst-case scenario is currently mitigated by the use of increased safety factors in space vehicle design. Nevertheless such a TPS oversizing limits the total payload, further increasing the overall cost.

Additionally to the boundary layer laminar-to-turbulent transitions, ablation phenomena add chemical reactions at the wall, as well as surface roughness and blowing; this work addresses mainly the effect of blowing, assessing the influence of continuous wall outgassing on boundary layer stability. Historically, Linear Stability Theory (LST) analyzed the interaction between blowing and boundary layer stability by focusing on the deformed mean flow, completely neglecting the perturbations originated by uneven blowing (see, for instance, by Malik[18]). The simplicity of this approach is still widely used nowadays (Johnson *et. al*[14] and Ghaffari *et al.*[13]).

More recently Fedorov[15] modeled the effect of pores on the second Mack's mode instability. Blowing was not considered, even if his development allows for it. This development is highly interesting for this application, mainly because experimental setups analyzing wall blowing are carried out very often by means of a porous wall. Unfortunately this is quite different from the outgassing originated by ablative wall pyrolysis because the whole surface expels gases, instead of small discrete and localized pores.

A complete simulation of the harsh hypersonic environment is very hard to achieve, primarily because of the complex interactions and concurrency of multiple phenomena. The high temperature reached in the flow triggers chemical reactions and species dissociation, not to mention wall catalysis. Experimental reproduction of the surface sublimation with a realistic boundary layer is difficult and, as a consequence, many setups achieve boundary layer

DOI: 10.13009/EUCASS2017-68

blowing by means of a porous surface. These experiments usually blow through the pores the same fluid used in the free stream, for instance air. Pyrolysis outgassing introduces new species with respect to the ones naturally available in dissociated air. Few experiments (as for instance the one reported by Fischer[6]) introduced different species into the boundary layer by means of a mock-up partially made of sublimating material. Unfortunately, Fischer closely mimicked only the presence of different species, while the density (and in general all the other properties) of the pyrolysis gas, together with the surface chemistry reactions, are not reproduced. Similarly, the faithful numerical reproduction of a hypersonic scenario tackling ablation, porosity and transition encounters many difficulties and it still represents a challenge. Furthermore, applications to real life vehicles would require a snappy tool able to influence early design decisions.

For this reason the use of Linear Stability Theory (LST), together with the eN method, is widely recognized as a sound and fast prediction method. Therefore an appropriate modeling of porous surface and blowing influence on the stability of boundary layers would be beneficial to the understanding of such a phenomenon.

In this regard, the difference between the blowing imposed by a porous surface and the one created by a surface sublimating at once is clear. The current work refers to these models respectively as *discrete* and *continuous* blowing to highlight the differences.

The present work will treat a continuous blowing surface, mimicking an ablative TPS wall, deriving a new set of boundary conditions. A comparison and a verification of these new boundary conditions have been realized in the LST solver available in the VESTA toolkit,[23] using a Chebyshev pseudo-spectral collocation method. The basic idea revolves around the design of a specific compatibility condition resulting from a simplification of the blowing mechanism. The current work deals with hypersonic flows around a flat plate with no pressure gradient. The effect on perturbation frequencies and growth rates is investigated in the following sections.

2. Governing equations

An unsteady laminar flow where only small perturbations are present can be easily decomposed in a steady and an unsteady part:

$$Q(x,y,z,t) = \overline{Q}(x,y,z) + q'(x,y,z,t)\,, \tag{1}$$

where Q is a generic flow variable. The mean flow $\overline{Q}$ is assumed to be steady, thus constituting the base flow on which the stability analysis is carried out. Perturbations $q'(x,y,z,t)$ are usually represented as mutually independent waves

$$q'(x,y,z,t) = \tilde{q}(y)\ \exp(i(\alpha x + \beta z - \omega t)) + c.c. \tag{2}$$

The perturbation amplitude $\tilde{q}(y)$ is dependent only on the wall normal coordinate as a direct consequence of the quasi-parallel flow assumption. Moreover, the latter hypothesis imposes no variation on any mean flow quantity along the streamwise and spanwise direction. As a consequence, vertical mean velocity is usually considered zero and it is actually negligible for a boundary layer flow.

These hypotheses are standard in the Linear Stability Theory (LST) analysis and they are usually associated with homogeneous boundary conditions. LST equations for compressible flows are abundantly reported in literature, as for instance by Mack[17] and Malik.[20] The version actually implemented in this work is not reported here for the sake of conciseness but it is the same as the one used by Pinna.[24] Such traditional system of equations cannot take into account the perturbations introduced in the boundary layer by the wall blowing, but it is naturally limited to the study of blowing effects on the mean flow, neglecting any unsteady behavior at the wall. On the other hand, in real applications, it is not possible to have an ideally even blowing: in order to take into account any irregularity in the wall blowing, boundary conditions need to be reconsidered.

Perturbations on the vertical velocity induced by a blowing wall are directly correlated with all the other disturbances at the wall and in the domain. For this reason, $\tilde{v}(0)$ must be treated as a function of all the other variables and it cannot be directly imposed as a Dirichlet boundary condition. As a matter of fact, such an assignment would change the nature of the system that would no longer be an eigenvalue problem. Two different boundary conditions modeling wall blowing are treated in the remaining of this work: a porous wall and a continuously sublimating wall.

All the equations are made non-dimensional with the usual LST reference quantities taken at the boundary layer edge: velocity U_e ,temperature T_e, and Blasius length $\ell = \nu_e \hat{x}/U_e$. Transport and other thermodynamic properties are evaluated considering the temperature at the boundary layer edge. For sake of clarity, the following naming convention is adopted hereafter: hat variables ($\hat{q}$) are dimensional and non-hatted variables (q) are non-dimensional, with the subindex w referring to wall variables.

DOI: 10.13009/EUCASS2017-68

2.1 Porous model

Blowing through a porous surface has been modeled by Gaponov et. al.[7–12] and Fedorov et. al.[5,16] The idea is to link the value of velocity perturbations to pressure ones at the wall through an admittance:

$$\tilde{v}(0) = K\tilde{p}(0). \tag{3}$$

The idea was also proposed by Carpenter & Porter[1] without giving a dependency of K on the porosity parameters. This dependency was obtained by Gaponov[8–10,12] and Fedorov[5] from the classic solutions of the Navier-Stokes equations describing acoustic waves traveling inside a long circular tube (see Daniels[3] and Gaponov[7]). The full derivation can be found in the aforementioned references and leads to Eqs. (4-10).

$$k_\nu = r\sqrt{\frac{i\,\omega\,\overline{\rho}_w}{\overline{\mu}_w}\,Re}\,, \tag{4}$$

$$Z_1 = \frac{i\,\omega}{\overline{T}_w}\,\frac{J_0(k_\nu)}{J_2(k_\nu)}\,, \tag{5}$$

$$Y_1 = -\,i\,\omega\,M_e^2\left(\gamma + (\gamma-1)\,\frac{J_2(\sqrt{Pr}\,k_\nu)}{J_0(\sqrt{Pr}\,k_\nu)}\right), \tag{6}$$

$$Z_0 = \sqrt{Z_1/Y_1}\,, \tag{7}$$

$$\Lambda = \sqrt{Z_1\,Y_1}\,, \tag{8}$$

$$n = \frac{S_{pores}}{S_{total}} = \frac{\pi\,r^2}{s^2}\,, \tag{9}$$

$$K = \frac{n}{Z_0}\,\tanh(\Lambda h)\,, \tag{10}$$

where r is the pore radius, s is the distance between pores, h is the porous layer height, n is the porosity, J_0 and J_2 are the Bessel functions of order 0 and 2, Z_1 is the impedance that characterizes the transmission line, Y_1 is the shunt admittance, Z_0 is the characteristic impedance and Λ is the propagation constant.

Note that these expressions were developed for porous coatings. The acoustic condition therefore considers that there is a hard impenetrable surface under the porous layer, thus assuming $\tilde{v}(-h) = 0$. This assumption is valid both for pyrolysing surfaces and blowing experiments. Pyrolysing surfaces will feature a porous layer on top of a composite layer with resin and fibres, thus being acceptable to assume the wall-normal velocity perturbation to be zero on it. Blowing experiments typically feature several porous layers with different sizes. Having one of these layers with very small pore radius, allows to assume $\tilde{v}$ to be zero on it.[12] This is usually the case, in order to stop the waves inside the blowing chamber from entering the wind tunnel. Therefore, the porous coating condition is, in any case, suitable for the considered porous wall configurations.

2.2 Continuous blowing model

A sublimating wall, whose outgassing is distributed over the surface itself, imposes a new balance at the wall and the impenetrability condition is no longer valid. Analogously to the porous case, a relation between the vertical perturbation velocity and all the other variables at the wall has to be found. For a distributed blowing it is less consistent to apply acoustic analogies, similar to what Gaponov did, as there are no localized cavities that expel gases. Regardless of the source of the wall perturbation, the linearized continuity equation has to be satisfied. Therefore it is possible to evaluate the linearized continuity equation at the wall. This operation is performed coherently to the well known y-momentum conservation manipulation, that have been already used to obtain the pressure compatibility conditions, as, for instance, shown by Malik.[19] The continuity equation:

$$\frac{\partial\rho}{\partial t} + \frac{\partial\rho U_j}{\partial x_j} = 0\,, \tag{11}$$

is linearized, simplified according to the LST assumptions and then evaluated at the wall. The resulting equation reads:

DOI: 10.13009/EUCASS2017-68

$$\overline{P}\,(-\overline{T}_y + \overline{T}\,\partial_y)\,\tilde{v} + (-i\,\omega\,\overline{T} - \overline{V}_w\,\overline{T}_y + \overline{V}_w\,\overline{T}\,\partial_y)\,\tilde{p} + \overline{P}\,(i\,\omega - \overline{V}_w\,\partial_y)\tilde{T} = 0. \tag{12}$$

Eq. (12) is then imposed as a boundary condition to obtain the normal velocity perturbation at the wall. This approach is similar to what is proposed by Mortensen[22] to study stability with ablation. In that case, continuity close to the wall, in the form of different surface mass balance conditions, is imposed to account for the wall ablation induced recession.

2.3 Limitations and inconsistencies

As already specified in section 2, LST comprises a number of assumptions to be respected. This clear theoretical framework supplements the limitations coming from classic boundary-layer theory. For this reason, the blowing velocity should not exceed a specific threshold: it shall be lower than $\overline{V}_w \sim 1/Re_\ell$. Where $\overline{V}_w$ is made non-dimensional by the boundary-layer streamwise velocity U_e and $Re_\ell = U_e\ell/\nu_e$. This does not prevent its application to practical cases with higher blowing rates, but a further validation against experimental data would be mandatory.

The introduction of a blowing velocity $\overline{V}_w$ in the base flow brings in an important inconsistency with respect to the aforementioned LST framework, regardless of the boundary condition used in the LST solver. This deviation is inherently linked to the parallel flow assumption; that is, the negligibility of variations along the streamwise and spanwise coordinates, i.e. $\overline{Q} \approx \overline{Q}(y)$. Such a hypothesis entails $\partial_x(\overline{\rho}\,\overline{U}) \approx 0$ and $\partial_z(\overline{\rho}\,\overline{W}) \approx 0$, which, through the continuity equation, also leads to $\partial_y(\overline{\rho}\,\overline{V}) \approx 0$ in the whole domain. This condition can be strictly satisfied either by requiring zero vertical velocity and corresponding derivatives

$$\overline{V} = \partial_y\overline{V} = 0, \tag{13}$$

imposing $\overline{V}(y = 0) = 0$ even if blowing or suction are present, or by making the product of the mean normal velocity and the mean density constant in all the domain:

$$\overline{V} = -C/\overline{\rho}. \tag{14}$$

In the latter case, the freestream $\overline{V}(y = \infty)$ is assumed to be $\overline{V}_w/\overline{\rho}_w$. Note that $\overline{V}_w$ and $\overline{\rho_w}$ are both non-dimensional. Classically, authors dealing with this inconsistency[13,14,18] have simply argued that since $\overline{V}_w << 1$, it is fair to assume Eq. (13). Boundary conditions imposed in this way are exactly the same with or without blowing and the only difference lies in the other mean flow variables ($\overline{U}$, $\overline{W}$, etc.). However, this assumption, even though it is satisfied when comparing the freestream velocity with the blowing velocity, it is not satisfied in the lower region of the boundary layer. As y approaches 0, $\overline{U}$ is reduced until, eventually, $\overline{U} \sim \overline{V}$.

Eq. (14) seems to be more consistent, since it allows for $\overline{V}(0) = \overline{V}_w$ and it also includes some decay of the normal velocity throughout the domain. However, this decay is not physically correct, since it is solely proportional to the density. This means that after the boundary layer limit δ, $\overline{\rho}(y > \delta) \approx 1$ and therefore $\overline{V}(y > \delta) \approx \overline{V}_w/\overline{\rho}_w$, rather than zero. This error would be present in the freestream region. The error introduced by Eq. (14) is expected to be smaller, since in the freestream region $\overline{V}$ would be much lower than 1, but, as a matter of fact, it would be simply spread over a larger region. Furthermore, the use of this assumption would need a new derivation of the stability equations. Many terms containing $\overline{V}$ would appear, requiring a major update of any existing stability code.

The present work proposes to treat the existing inconsistency by modeling the normal velocity $\overline{V}(y)$ with a discontinuous function:

$$\overline{V}(y) = \begin{cases} \overline{V}_w & y = 0 \\ 0 & y > 0 \end{cases}. \tag{15}$$

Moreover, the derivatives of the normal velocity with respect to the normal coordinate $\overline{V}_y$ and $\overline{V}_{yy}$ are considered zero in all the domain. The main advantage of this approach is that classic LST codes can be used without any major modification aside from the boundary condition, and still keep a good representation of the normal velocity in the region close to the wall. Nevertheless, it is not free from error. The discontinuous definition of the velocity means that the continuity equation applied on the mean variables at the wall will not be satisfied, since $\partial_y(\overline{\rho}\,\overline{V}) = \overline{V}_w\,\partial_y\overline{\rho} \neq 0$.

The implementation inside the VESTA toolkit[23,25] was achieved by simply modifying the boundary conditions. Aside from the additional boundary condition in Eq. (12), modeling the non-zero normal velocity perturbation, the compatibility condition on the pressure perturbation at the wall will have to be modified to account that $\overline{V}_w \neq 0$:

DOI: 10.13009/EUCASS2017-68

$$\left(\frac{i\,\omega\,t_{1,w}}{\overline{T}_w} - \frac{\beta^2\,\overline{\mu}_w}{Re} - \frac{\overline{\mu}_w\,\alpha^2}{Re} + \left(-\frac{\overline{V}_w\,t_{1,w}}{\overline{T}_w} + \frac{2\overline{\mu}_{\overline{T},w} + \overline{\lambda}_{\overline{T},w}}{Re}\,\overline{T}_{y,w}\right)\partial_y + \frac{\ell_{2,w}\,\overline{\mu}_w}{Re}\,\partial_{yy}\right)\tilde{v} + \\ + \frac{\ell_{1,w}\,\overline{\mu}_w}{Re}\,(i\beta\,\partial_y\tilde{w} + i\,\alpha\,\partial_y\tilde{u}) - \partial_y\tilde{p} + \frac{\overline{\mu}_{\overline{T},w}}{Re}\,(i\beta\,\overline{W}_{y,w} + i\,\alpha\,\overline{U}_{y,w})\,\tilde{T} = 0, \quad (16)$$

where $t_{1,w} = \gamma M_e^2 \overline{P}_w$, $\ell_{1,w} = 1 + \overline{\lambda}_w/\overline{\mu}_w$ and $\ell_{2,w} = 2 + \overline{\lambda}_w/\overline{\mu}_w$.

Quantifying the error committed by each of the possible approaches is not trivial. The first approach (Eq. (13)) introduces an error of the order $\overline{V}_w \sim 1/Re_\ell$ (see Cebeci & Cousteix[2]) in the boundary $y = 0$. The second one (Eq. (14)) also introduces an error of order $\overline{V}_w \sim 1/Re_\ell$ but in the region $y > \delta$. The proposed approach (eq. 15) does not introduce an error in the boundary values, but unlike the others, it does not respect the continuity equation in the proximity of $y = 0$, which introduces an error of order $\overline{V}_w\,(\partial_y\overline{\rho})_w \sim (\partial_y\overline{\rho})_w/Re_\ell$.

Both approaches introduce an error, however it is reasonable to expect that the proposed approach (Eq. (15)) approximates reality more accurately, since both the boundary conditions are respected, and the disagreement of the continuity condition is not very significant (values of $(\partial_y\overline{\rho})_w$ are typically around $10^{-6} - 10^{-4}$ for hypersonic boundary layer).

3. Verification and validation

The current implementation is compared against Gaponov & Ermolaev's experimental and LST results.[11] This test case is for a 44 cm flat plate with no pressure gradient in a cold hypersonic flow. The corresponding condition are presented in Tab. 1. The coating is experimentally applied between 50 mm and 170 mm. In Fig. 1, the amplification factor is plotted against the position along the surface x. The amplification factor A is defined as:

$$\frac{A(x)}{A_0} = \exp\left(\int_{x_0}^{x} -\alpha_i\,(\xi)\;d\xi\right), \quad (17)$$

where A_0 is the amplitude of the perturbation at $x_0 = 70$ mm which is fixed to 1.

Two cases are plotted with the same porosity $n = 0.39$, the same pore radius $\hat{r} = 5\,\mu$m and two different values of the porous-layer height $\hat{h} = 0.4$ mm and $\hat{h} = 2.5$ mm. As one can see, the agreement between the LST calculation is excellent. It is worth noting that the amplitude retrieved experimentally departs from the theoretical curve producing a much sharper increase in the growth rates. This difference is caused most probably by the appearance of the later stages of transition, not captured by the linear theoretical model.

$Re_{1,e}\left[\mathrm{m}^{-1}\right]$	M_e	Pr	T_e [K]	$\beta\left[\mathrm{mm}^{-1}\right]$	$\hat{F}$ [kHz]
6.6×10^6	2	0.72	161.11	0.22	10

Table 1: Flow parameters in the experiments, and the LST simulations performed by Gaponov & Ermolaev.[11]

4. Results

Several tests are performed with the two different boundary conditions. The porous boundary condition depends on 3 different parameters: pore radius, porosity and porous layer height. According to a preliminary set of calculations, porosity n (Eq. (9)) seems to be the least important, even though not entirely negligible. The influence of this parameter on a Mach 4.5 calculation is shown in Fig. 2. Despite the fact porosity is not completely negligible, its effect on the growth rate is considerably lower than the one obtained from the pore radius and the porous-layer height (see the analysis of Miró[21]). For this reason, porosity is not investigated any further in this paper and is kept constant at $n = 0.8$.

The actual process leading to the creation of a porous material can vary significantly, thus leading to different sizes and distribution types. In the current work four different height and radii, shown in Tab. 2, have been chosen to carry out a parametric study. Mean flows are retrieved by means of a self-similar solution, according to the condition reported in Tab. 3. Wall blowing has been computed with a self similar solution. Albeit this may not be directly representing a real application, it allows to study in greater detail the physics, with limited computational resources. The natural implication is that the actual blowing velocity decreases with the Reynolds number, because of the constant

DOI: 10.13009/EUCASS2017-68

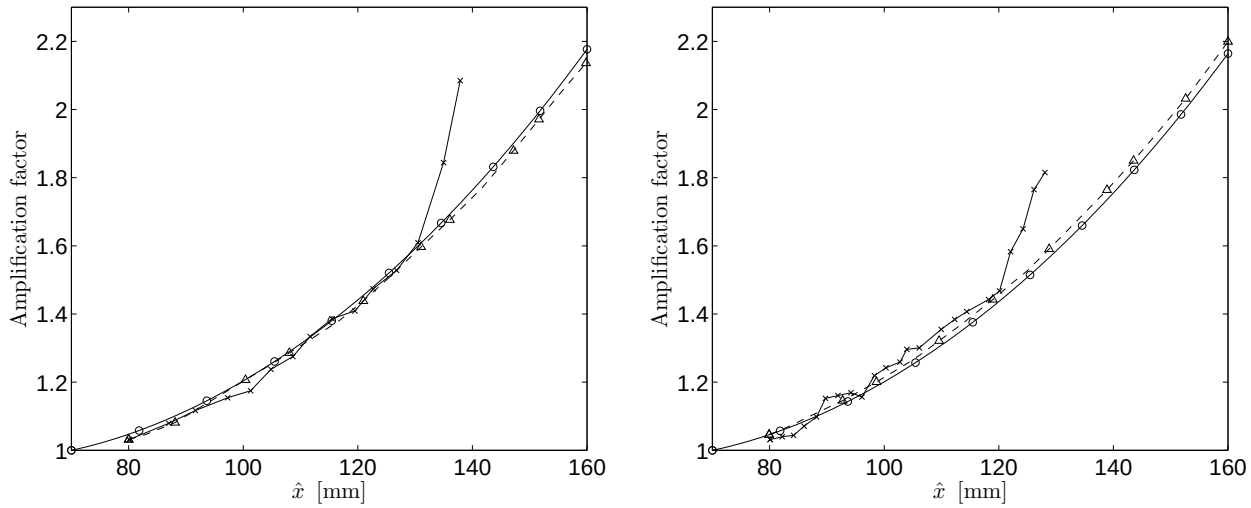

(a) $n = 0.39$, $\hat{r} = 5\,\mu$m & $\hat{h} = 0.4$ mm (b) $n = 0.39$, $\hat{r} = 5\,\mu$m & $\hat{h} = 2.5$ mm

Figure 1: Comparison between the experimental, and LST results obtained by Gaponov & Ermolaev[12] against VESTA's LST results. The flow conditions are those in Tab. 1. —○— LST VESTA toolkit, —×— Gaponov & Ermolaev[12] experiments, - -△- - Gaponov & Ermolaev[12] LST.

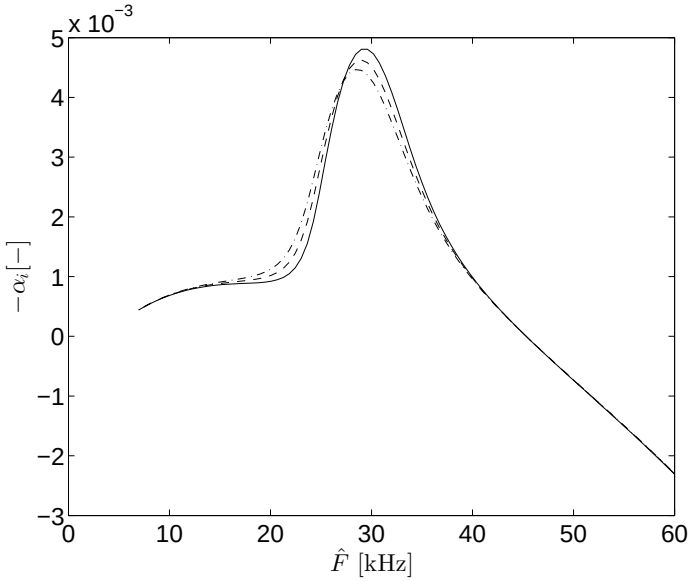

Figure 2: Influence of the porosity on stability for a case with porous coating ($\hat{r} = 0.05$mm & $\hat{h} = 0.4$mm) and for the flow conditions $\rho_e = 1.899 \times 10^{-2}$ kg m^{-3}, $Pr_e = 0.72$, $M_e = 4.5$, $T_e = 61.61$ K, $\hat{T}_w = 311$ K, $\gamma = 1.4$, with $Re_\ell = 1500$. —— $n = 0.6$; - - - - $n = 0.8$; —·— $n = 0.99$

	h1	h2	h3	h4
$\hat{h}$ [mm]	5	3.5	3	0.5
$\hat{r}$ [mm]	5	3.5	3	0.5

Table 2: pore radius and height used for all the simulations

DOI: 10.13009/EUCASS2017-68

Case	Mach	Re_ℓ	$\hat{T}_\infty$ [K]	$\hat{p}_\infty$ [Pa]	B
A	6	2000	70	4000	2.828e-05
B	8	2000	70	4000	2.828e-05

Table 3: Flow conditions for the mean flow calculations

value of the Blasius function at the wall. On the other hand, a more realistic blowing, mimicking an ablative material, would not decrease the wall blowing speed according to the Reynolds number. In such a situation the effect on the transition onset would depend also on the blowing intensity at previous locations; boundary layer history will not be addressed in the current paper. In the current work the blowing velocity for the Mach 6 and Mach 8 flat plate simulation has been derived from the value $f_w = -0.04$. The non-dimensional wall blowing velocity is linked to the value of the Blasius function at the wall by means of the relation

$$f_w = K\, Re_\ell\, \rho_w \overline{V}_w\,, \tag{18}$$

where, for a flat plate, $K = -1/\sqrt{2}$. For the Mach 6 case, this corresponds to a dimensional velocity $\overline{V}_w = 0.1974\,\mathrm{m/s}$. It is worth noting the compatibility of the blowing magnitude with the theoretical limitations of the model shown in sec. 2.3. In order to represent the blowing with respect to the free stream it is convenient to introduces as well a non-dimensional blowing parameter:

$$B = \frac{\hat{\rho}_w \hat{v}_w}{\rho_e U_e}\,, \tag{19}$$

which represents a mass flux for equivalent surfaces. This is useful to scale similarly different blowing in different freestream conditions. In this work the blown fluid will be the same than the free stream one, nevertheless for denser pyrolysis gases, the higher density will disturb more the incoming flow. Denser must not be confused with heavier (higher molecular weight), since Stalmach et al.[26] reported that it is the lighter blowing gases that have a stronger destabilizing effect. The blowing parameter is linked to the Blasius function at the wall by

$$B = \frac{f_w}{K\, Re}\,, \tag{20}$$

where $K = -1/\sqrt{2}$ for a flat plate. The fluid considered in this work is air with a constant Prandtl number $Pr = 0.7$, a specific heat ratio $\gamma = 1.4$ and a gas constant $R = 287.05\,\mathrm{J\,kg^{-1}\,K^{-1}}$. The specific heat at constant pressure $c_p = 1004.5\,\mathrm{J\,kg^{-1}\,K^{-1}}$. Viscosity is computed with Sutherland's law

$$\hat{\mu} = \hat{\mu}_{ref} \left(\frac{\hat{T}}{\hat{T}_{ref}} \right)^{3/2} \frac{\hat{T}_{ref} + \hat{S}}{\hat{T} + \hat{S}}\,, \tag{21}$$

using $\hat{\mu}_{ref} = 1.716 \times 10^{-5}\,\mathrm{Pa\,s}$, $\hat{S} = 110.6\,\mathrm{K}$, $\hat{T}_{ref} = 273.15\,\mathrm{K}$; bulk viscosity is estimated by mean of the Stokes hypothesis. The small blowing velocity used in this work triggers only a small modification in the mean flow as visible in Fig. 3(b). If the perturbation velocity is assumed to be zero, $\tilde{v}(0) = 0$, that is no special boundary condition is applied to the solver, only minor differences are expected on the mean flow stability. Fig. 3(a) confirms this trend only for the first Mack mode, showing growth rates calculated with a homogeneous vertical velocity boundary condition lying close to the ones obtained for a flow without any blowing. Second Mack mode, instead, has its peak displaced at lower frequencies with higher growth rates. Despite the fact that this is a very common approach, this case represents an ideal set up rather than a realistic one, where wall blowing is a further source of flow perturbation. Because of its ideal nature this case represents a valid benchmark in the analysis of the different boundary conditions. The growth rate peaks appear around 411 kHz for the blown boundary layer and at 428 kHz for the case with zero imposed velocity at the wall.

If the corresponding boundary layer blowing is introduced by means of a porous layer, the growth rate of the unstable frequencies varies considerably. The mean flow is still the one presented in Fig. 3(b), leading to the growth rates in Fig. 4 for different arrangement of the porous layer. In Fig. 4(a) the smallest height is taken while comparing the four different radius sizes. Smaller radii smooth down the peaks, shift them to lower frequencies and lower the peak height. On the other hand, between different radii, the peak shift remains almost constant moving to 173 kHz for a big radius and 166 kHz for a small one. A second peak lying approximately around 400 kHz appears also with the porous boundary condition: or the biggest radii its growth is comparable to the boundary layer without blowing while, for the smallest radius r4 it is slighlty damped, consistently to what observed for the first dominant peak. Fig. 4(b) shows that perturbations become more unstable for shallower porous layers. Several peaks occur in the diagram for bigger layer

DOI: 10.13009/EUCASS2017-68

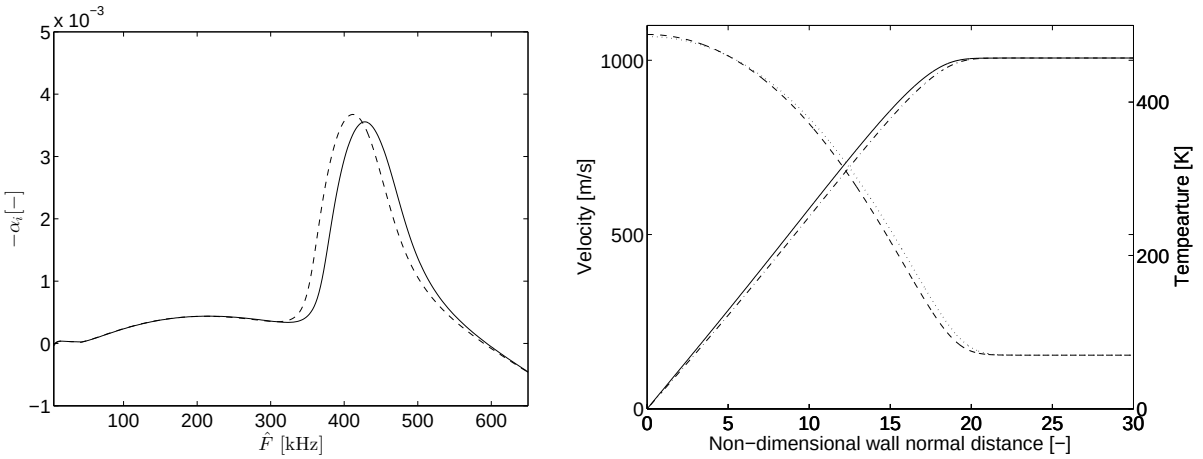

(a) (b)

Figure 3: Growth rates for a Mach 6 flat plate with and without blowing with $\tilde{v}(0) = 0$. Flow conditions are taken for case A in Tab. 3: ——, no-blowing; - - - - $f_w = -0.04$.(left) Mach 6 profiles: —— velocity no-blowing; —·—, velocity $f_w = -0.04$, - - - -, temperature no-blowing; ·····,temperature $f_w = -0.04$. (right)

heights (h1, h2, h3), while for the shallowest one (h4) the peak distribution shows only two peaks with one of them at a similar frequencies than the second Mack mode for the no-blowing case.

The many peaks found for bigger pore height have a growth comparable with the second Mack mode obtained with homogeneous wall perturbation, even though it is generally lower. For the smallest height possible the growth rate increases considerably, reaching values approximately one order of magnitude bigger than the first Mack mode that would naturally peak around those frequencies, if obtained with the homogeneous boundary condition. On the other hand, with respect to the second Mack mode, the enhanced growth rate corresponds to, approximately 30% of the no-blowing case. It should be noted that the growth rate level increased approximately of one order of magnitude. Unlike the effect of pore radius, larger porous layer heights shift considerably the frequency of the most unstable mode, from slightly above 200 kHz down to 166 kHz. More interestingly, for higher porous layers a series of peaks of comparable sizes appears at lower frequencies, while only one is visible for the h4 case. Results obtained for a porous surface without blowing provide a very similar trend of the growth rates. Similarly to Fig. 3(a) the little blowing is so small that the effect of the mean flow profile is rather small.

A comparison between the porous model and the continuous blowing one proposed in this paper is available in Fig. 5, where it is possible to observe that a continuous blowing displays a further shift of the peak at an even lower frequency while retaining, at least in this case, a similar growth rate. In terms of peak height and peak shift it is interesting to note that the porous wall boundary condition tends to return growth rates similar to the continuous blowing one. The most important difference lies in the absence of multiple peaks and the wider range of highly unstable frequencies. While difficult to verify experimentally, such a difference remains reasonable because, unlike the boundary condition proposed by Gaponov, there is no acoustic coupling. It has been already found by Miró[21] that the two boundary conditions get closer and closer as the pore dimensions keep increasing, reaching practically the same value for $\hat{r} = 10\,\text{mm}$ and $\hat{h} = 10\,\text{mm}$.

Obviously the Mach number plays a significant role in the growth rate of the disturbances. The test performed used the condition of case B in Tab. 3. Fig. 6(a) shows an interesting drop of the instability for Mach 8. This is visible as well in Fig. 6(b), where the same mean flow is used but the pores are considered much smaller. For smaller pore radius and height, the peak is shifted toward higher frequencies.

A comparison of the behavior of the continuous boundary condition at different Mach number is shown in Fig. 7. This figure reports as well a Mach 8 calculation performed on a profile obtained with $f_w = -0.05$. The tiny difference in the profile produces a small difference also in the growth rate. Even when using the continuous blowing boundary condition, a Mach number increase tends to stabilize the flow. On the other hand the shift in frequency is more limited, despite being always present.

5. Conclusion

An analysis of the newly implemented boundary conditions inside VESTA toolkit has been discussed. The implementation of a porous boundary condition has been successfully verified against experiments and other implementations

DOI: 10.13009/EUCASS2017-68

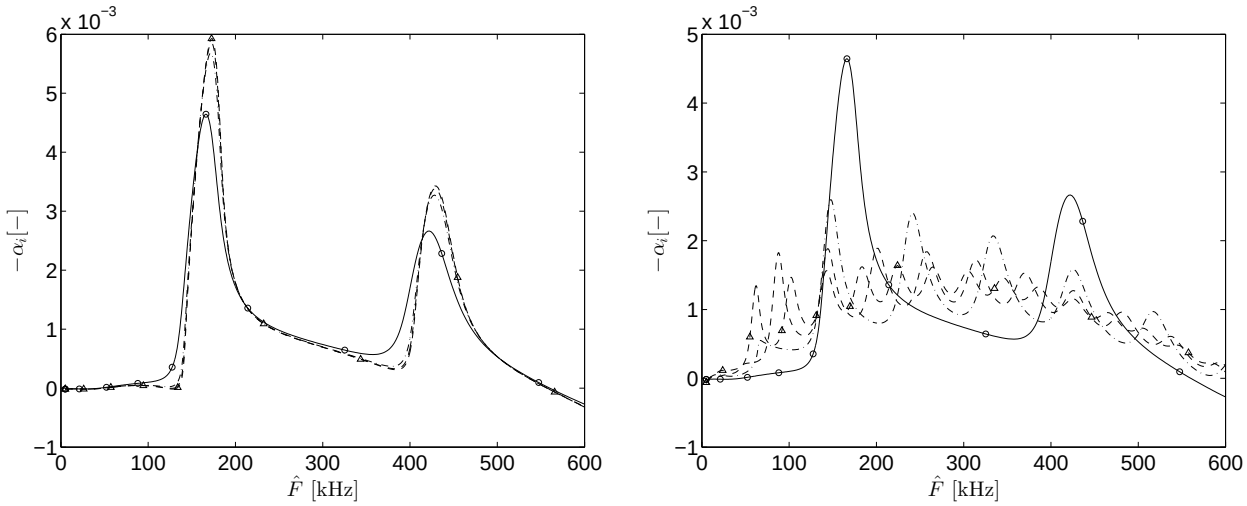

(a) Analysis of radius influence for the smallest porous layer height h4: -△-, r1; - - -, r2; —·— r3, —○— r4.

(b) Analysis of height influence for the smallest pore radius r4: -△-, h1; - - -, h2; —·— h3, —○— h4.

Figure 4: Effect of porous height and radius for a Mach 6 flat plate

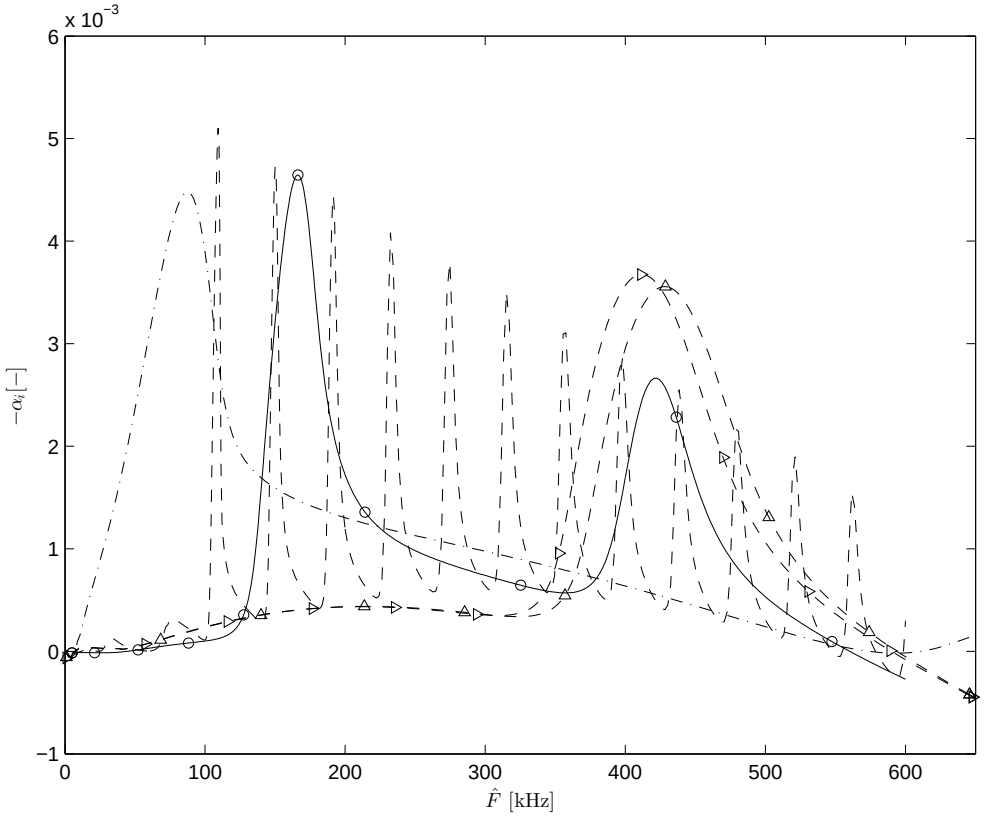

Figure 5: Growth rates for a Mach 6 flat plate comparing all different boundary conditions. Flow conditions are taken for case A in Tab. 3. -△- homogeneous b.c., no blowing; -▷- homogeneous b.c. $f_w = -0.04$; —·— continuity b.c., $f_w = -0.04$; - - - - porous b.c., radius r1, height h1; —○— porous b.c., radius r4, height h4

DOI: 10.13009/EUCASS2017-68

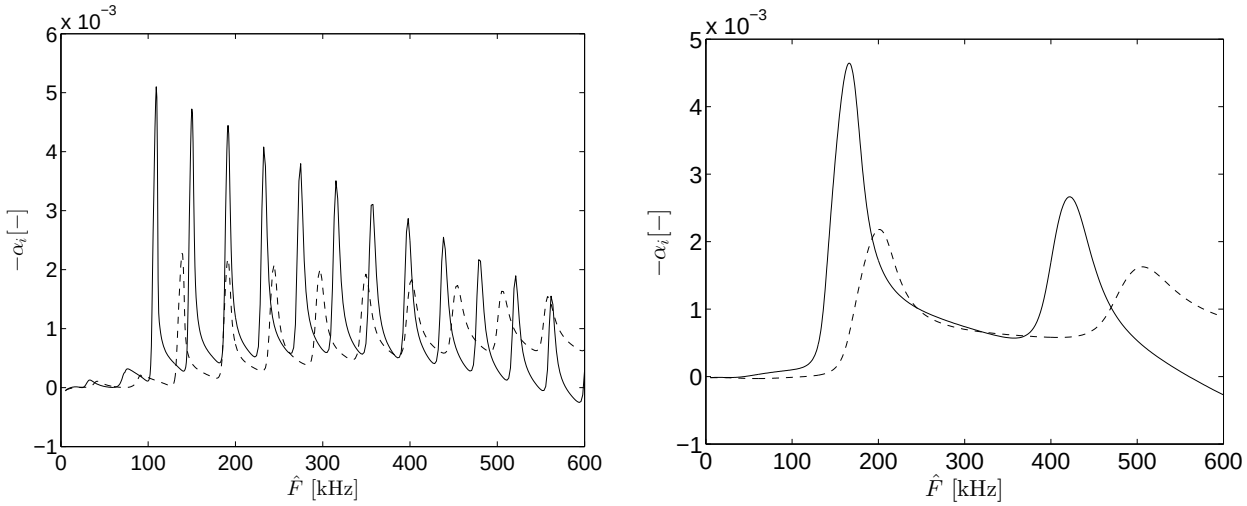

Figure 6: Comparison of Mach 6 and Mach 8 growth rate for a porous boundary condition for the biggest radius and height (on the left) and smallest radius and height (right). - - - - Mach 8 $f_w = -0.04$, —— Mach 6 $f_w = -0.04$

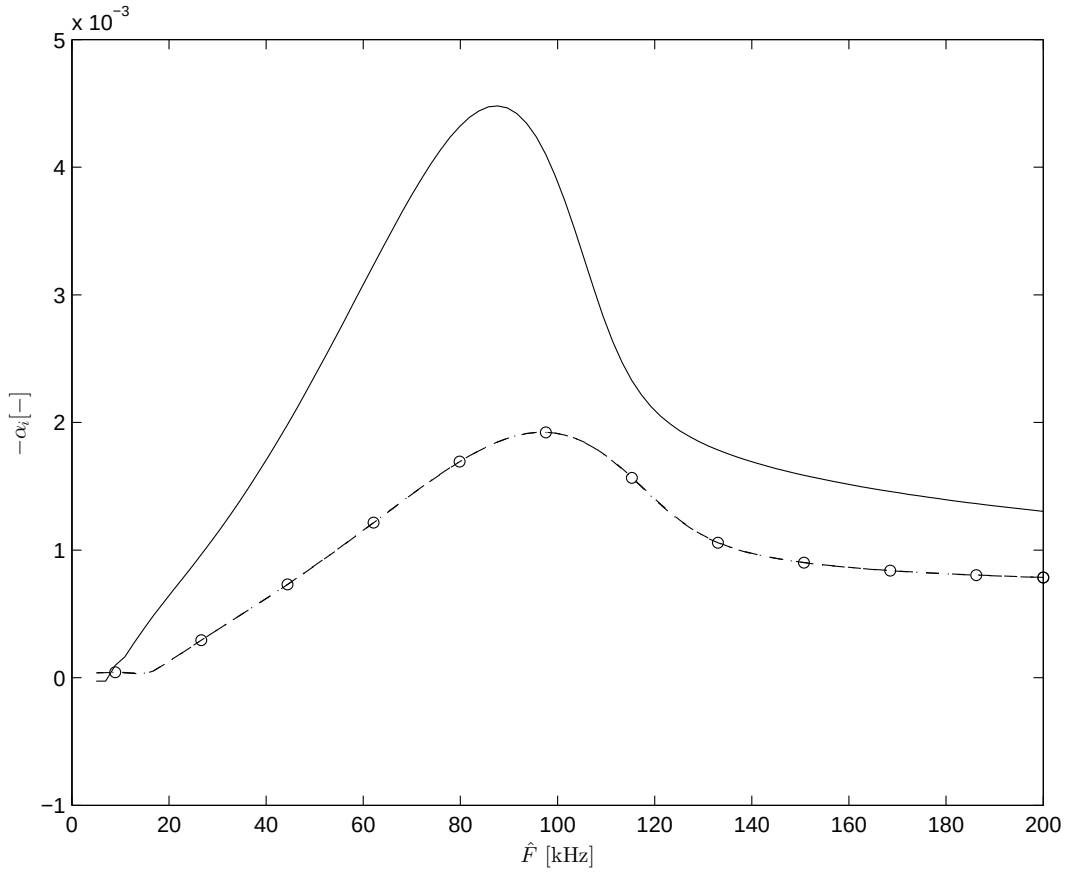

Figure 7: Comparison between Mach 6 and Mach 8 growth rates for at Re 2000 for a continuous blowing boundary condition. - - - - Mach 8 $f_w = -0.04$, —○— Mach 8 $f_w = -0.05$, —— Mach 6 $f_w = -0.04$

DOI: 10.13009/EUCASS2017-68

reported in literature. Furthermore a new boundary condition reproducing the outgassing of a pyrolysing surface has been developed. Despite the lack of experimental evidence, due to the difficulty of performing such experiments, the two boundary conditions have been found to agree on their basic behavior.

The present work found that both models provided a substantial increase of the growth rate peaks with a shift of the corresponding frequencies toward higher values. Such a shift is always present even when a simple homogeneous boundary condition is considered, and it could be partially linked to the different boundary layer thickness induced by the wall vertical velocity. On the other hand the stronger shift displayed with the two models discussed in the present work is linked to the actual behavior of the perturbation.

It is found that the two boundary conditions return similar results once the porous layer has big enough pores. In the work of Miró[21] such an equivalence is found for pores with a radius and height of 10 mm.

The present cases show that a smaller enhancement of the instabilities is associated with a growing Mach number. On the other hand, calculations at lower Mach number reported by Miró showed a smaller growth rate peak in comparison to what has been found in this work for Mach 6 and Mach 8. Therefore a more systematic study on the Mach number should be carried out to fully characterize these boundary condition with respect to that parameter.

References

[1] P. W. Carpenter and Porter L. J. Effects of passive porous walls on boundary-layer instability. *AIAA Journal*, 39(4), 2001.

[2] Tuncer Cebeci and Jean Cousteix. *Modelling and Computation of Boundary Layer Flows*. Springer, 1999.

[3] F. B. Daniels. On the propagation of sound waves in a cylindrical conduit. *Journal of the Acoustical Society of America*, 22:563, 1950.

[4] B. Elison and B.W. Webb. Local heat transfer to impinging liquid jets in the initially laminar, transitional, and turbulent regimes. *International Journal of Heat and Mass Transfer*, 37(8):1207–1216, 1994.

[5] A. V. Fedorov and N. Malmuth. Stabilization of hypersonic boundary layers by porous coatings. *AIAA Journal*, 39(4):605–610, 2001.

[6] M. C. Fischer. An experimental investigation of boundary-layer transition on a 10° half-angle cone at Mach 6.9. Technical Report TN D-5766, NASA, 1970.

[7] S. A. Gaponov. Effect of the properties of a porous coating on the boundary layer stability. *Izevestia SO AN SSSR, Seria Technicheskich Nauk*, 3(1):21 (in Russian), 1971.

[8] S. A. Gaponov. Influence of porous layer on boundary-layer stability. *Izevestia SO AN SSSR, Seria Technicheskich Nauk*, 1(3):21–23 (in Russian), 1971.

[9] S. A. Gaponov. Influence of gas compressibility on stability of boundary layer on porous surface at subsonic speeds. *Zhurnal Prikladnoi Mechaniki i Technicheskoi Fiziki*, 1:121–125 (in Russian), 1975.

[10] S. A. Gaponov. Stability of supersonic boundary layer on porous wall with heat conductivity. *Izevestia AN SSSR, Mechanika Zhidkosti i Gaza*, 3:41–46 (in Russian), 1977.

[11] S. A. Gaponov and Y. G. Ermolaev. Influence of porous-coating thickness on the stability and transition of flat-plate supersonic boundary layer. *Thermophysics and Aeromechanics*, 19(4):555–560, 2012.

[12] S. A. Gaponov and N. M. Terekhova. Controlling supersonic boundary layer stability by means of distributed mass transfer through a porous wall. *Fluid Dynamics*, 48(6):761–772, 2012.

[13] Shirin Ghaffari, Olaf Marxen, Gianluca Iaccarino, and Eric S. G. Shaqfeh. Numerical simulations of hypersonic boundary-layer instability with wall blowing. *48th AIAA Aerospace Sciences Meeting*, 2010.

[14] Heath B. Johnson, Joel E. Gronvall, and Graham V. Chandler. Reacting hypersonic boundary layer stability with blowing and suction. *47th AIAA Aerospace Sciences meeting*, 2009.

[15] V. F. Kozlov, A. V. Fedorov, and N. D. Malmuth. Acoustic properties of rarefied gases inside pores of simple geometries. *Journal of the Acoustical Society of America*, 117(6):3402–3412, 2005.

[16] S. V. Lukashevich and A. V. Fedorov. Stabilization of high-speed boundary layer using porous coatings of various thicknesses. *40th AIAA Fluid Dynamics Conference*, 2010.

DOI: 10.13009/EUCASS2017-68

[17] L. M. Mack. Boundary layer linear stability theory. Technical Report 709, AGARD, VKI, Brussels, 1984.

[18] M. R. Malik. Prediction and control of transition in supersonic and hypersonic boundary layer. *AIAA Journal*, 27(11):1487–1493, 1989.

[19] M. R. Malik. Numerical methods for hypersonic boundary layer stability. *Journal of Computational Physics*, 86(2):376–413, 1990.

[20] M. R. Malik. Stability theory for chemically reacting flows. In D. Arnal and R. Michel, editors, *IUTAM Symp. "Laminar-Turbulent Transition"*. Springer Verlag, Toulouse, 1990.

[21] F. Miró Miró. Numerical study of the stability of a hypersonic boundary layer in the presence of blowing. Technical Report 2015-28, von Karman Institute for Fluid Dynamics, Rhode-Saint-Genèse, Belgium, 2015.

[22] Clifton H. Mortensen and Xiaolin Zhong. Real gas and surface ablation effects on hypersonic boundary layer instability over a blunt cone. *43rd Fluid Dynamics Conference, American Institute of Aeronautics and Astronautics*, 2013.

[23] F. Pinna. VESTA toolkit: a Software to Compute Transition and Stability of Boundary Layers. *43rd AIAA Fluid Dynamics Conference, San Diego, California*, 2013.

[24] F. Pinna. Stability of boundary layer flows in different regimes. In *Progress in Flow Instability Analysis and Laminar-Turbulent Transition Modeling*. Von Karman Institute for Fluid Dynamics, 2014.

[25] F. Pinna and K. Groot. Automatic derivation of stability equations in arbitrary coordinates and for different flow regimes. *43th AIAA Fluid Dynamics Conference, Atlanta*, 2014.

[26] C. J. Stalmach, J. J. Bertin Jr., and T. C. Pope. A study of the boundary layer transition on outgassing cones in hypersonic flow. Technical Report NASA CR-1908, Vought Aeronautics Company/NASA Langley Research Center, Washington D.C., December 1971.